International Forum on Aeroelasticity and Structural Dynamics
IFASD 2024
17-21 June 2024, The Hague, The Netherlands

DECENTRALIZED CONTROL OF AILERONS FOR GUST LOAD ALLEVIATION

K. Michel[1], S. Schulz[1], G. Looye[1], G. Weber[2]

[1]DLR, Institute of System Dynamics and Control
Münchener Str. 20, 82234 Weßling, Germany
kolja.michel@dlr.de
simon.schulz@dlr.de
gertjan.looye@dlr.de

[2]Liebherr-Aerospace Lindenberg GmbH
Pfänderstr. 50-52, 88161 Lindenberg, Germany
guido.weber@liebherr.com

Keywords: Decentralized control, gust load alleviation, GLA, flexible aircraft, optimization

Abstract: This paper describes the design of a so-called decentralized gust load alleviation system for an aircraft with high aspect ratio wings. The system uses control loops at each individual aileron actuator that aim to reduce local structural dynamics at each respective point of installation in the wing structure. To this end, each actuator is equipped with a remote electronic unit that incorporates an inertial measurement unit and a processing unit that allows for implementation of a fast, local control loop that combines control surface positioning with local structural damping. At an aircraft level, this renders a decentralized control structure. Although the number of design degrees of freedom is lower than for a centralized system, over-all system complexity is considerably reduced. The presented design shows that remarkable improvement of structural damping and reduction of wing root bending moments can be achieved.

1 INTRODUCTION

One objective for future aircraft is a further improved fuel efficiency. This can be achieved by reducing the drag of the wings, which in turn is achieved by increasing the wing aspect ratio and span. This results undesirably in higher loads, e.g., bending moments, during gust encounters. In order to have slender wings and not increase the structural weight, the loads must be reduced in other ways. This can be achieved by means of active Gust Load Alleviation (GLA).

Various methods have already been implemented in the past and some of them are also used in commercial aircraft [1]. If available, this load reduction functionality is usually executed on the central flight control computer (FCC). The FCC accesses then the measurement data from distributed sensors and controls various control surfaces.

A common principle for active structural damping in other areas of application is collocated control, where the sensor is located close to the actuator position, enabling a reaction directly on site [2]. In [3] a concept of Remote Electronic Units (REUs) located close to the aileron actuators is proposed. These receive the control commands from the FCC, but also measure the accelerations on site and can locally process control laws (Fig. 1). This allows the application of a decentralized gust load alleviation system for large passenger aircraft with a possibly lower effort of integration.

The objective of this paper is to simulatively investigate this concept and design control laws for the REUs, allowing them to react locally and independently of each other to the gust-induced accelerations on the wing with control surface deflections. It is to see to which extent the movement of the wing can be dampened and thereby the wing root bending moment can be reduced.

For this purpose, a simple and robust control scheme is designed and optimized with respect to performance and stability criteria. The closed loop system consists of the dynamic flexible aircraft model, the actuator dynamics and the multiple local control loops. The dynamic flexible aircraft model represents the rigid body as well as flexible dynamics of the aircraft for multiple flight points and aircraft configurations. The model enables the calculation of the internal loads acting on the airframe during the encounter of atmospheric disturbances. Then, within this environment the optimization of the control parameters is performed. With the resulting parameters the decentralized control is simulatively evaluated.

In the upcoming Section 2 the concept of the decentralized control will be explained with more details. Then, in Section 3 the modeling of the flexible aircraft for control design is presented. Section 4 describes the optimization process and the defined quality criteria. It is followed by Section 5 with the results and a conclusion in Section 6.

2 CONCEPT OF THE DECENTRALIZED CONTROL

The concept of decentralized control for gust load alleviation consists of remote electronic units positioned near the aileron actuators. These are equipped with inertial measurement units (IMU) for acceleration measurement and a processing unit. This allows control laws to be implemented and executed locally on the REUs, resulting in increased sampling rates and reduced delays. These decentralized control loops are locally counteracting the gust induced acceleration of the wing by deflecting the corresponding aileron. [3, 4]

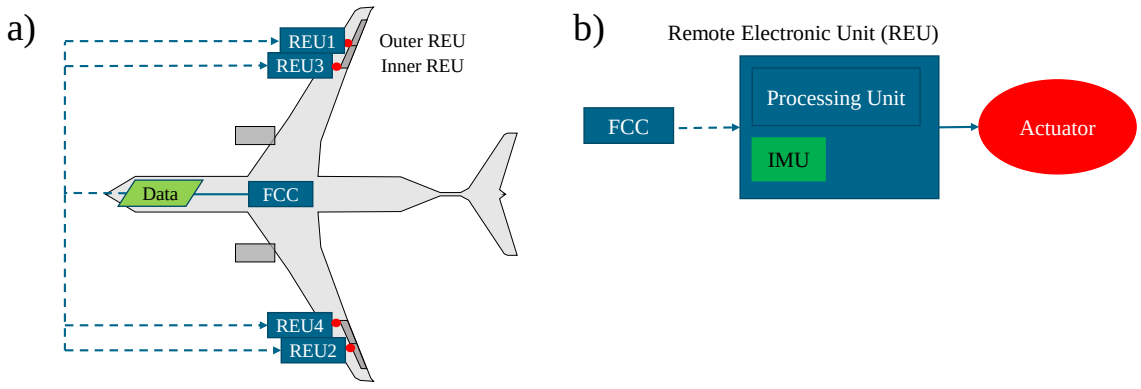

Figure 1: REUs on aircraft and schematic of REU

Figure 1 shows the concept in a simplified form. The assumed architecture consists of a wing with four ailerons (two on each side), each equipped with an REU near the actuator (see Fig. 1 a)). The REUs receive commands (primary flight control) from the flight control computer and also execute the decentralized control for load reduction. A schematic of the REU can be seen in Figure 1 b). The processing unit can operate the control at a sampling rate of up to 1000 Hz, whereby the FCC (typically 100 Hz) can be avoided for the fast GLA control loop.

3 MODELING OF THE AIRCRAFT FOR CONTROL DESIGN

For controller design and validation a model of the flexible aircraft and the other components involved is required. These are combined in Matlab Simulink. A central component here are the control synthesis models of the flexible aircraft model, which are described in the Sections 3.1 and 3.2. Figure 2 shows a schematic of the controller synthesis environment. The control system consists of an actuator model, the model of the flexible aircraft and the modeling of the sensor dynamics. The control loop is closed by the local control laws of the decentralized control system. The disturbances in the system are symmetrical gusts (see Section 3.1.2) that hit the trimmed aircraft model.

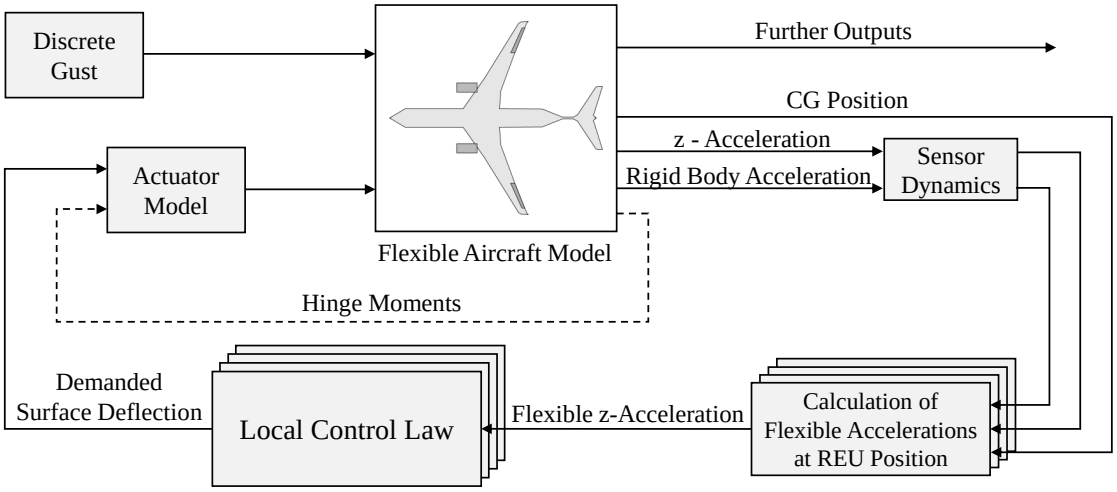

Figure 2: Scheme of the controller synthesis environment

The flexible aircraft model provides various outputs for evaluation, as well as for direct use in the control loop. The z-accelerations of the flexible wing are required for decentralized control in the REUs. Together with the rigid body acceleration and the position of the center of gravity of the aircraft, the flexible z-accelerations are calculated for each REU, which are then required in the local controls on the REU (see sec. 4.1). The sensor dynamics are represented here by a delay of 5 ms. The demanded surface deflection calculated by the control law is processed by an actuator model. Its output is then fed back into the flexible aircraft model. A simplified second-order actuator model without load dependency is used for controller synthesis. The high fidelity model from Liebherr-Aerospace, which is described in Section 3.3, is then used for the final evaluation. The components described here are explained in detail below.

3.1 Modeling of the flexible aircraft

The optimization of the control laws requires a flexible dynamic aircraft model capable of representing the rigid body dynamics of the whole aircraft and the structural dynamics of the airframe. This model is derived using the *VarLoads* framework [5]. The rigid body dynamics and structural dynamics of the flexible aircraft are represented by the following equations of motion

$$\begin{bmatrix} m_\mathrm{b}\left(\dot{\boldsymbol{v}}_\mathrm{b} + \boldsymbol{\omega}_\mathrm{b} \times \boldsymbol{v}_\mathrm{b} - \boldsymbol{T}_\mathrm{bE} \cdot \boldsymbol{g}_\mathrm{E}\right) \\ \boldsymbol{J}_\mathrm{b}\boldsymbol{\omega}_\mathrm{b} + \boldsymbol{\omega}_\mathrm{b} \times \left(\boldsymbol{J}_\mathrm{b}\boldsymbol{\omega}_\mathrm{b}\right) \end{bmatrix} = \boldsymbol{\Phi}_\mathrm{gb}^\mathrm{T} \boldsymbol{P}_\mathrm{g}^\mathrm{ext} \tag{1a}$$

$$\boldsymbol{M}_\mathrm{ff}\ddot{\boldsymbol{u}}_\mathrm{f} + \boldsymbol{B}_\mathrm{ff}\dot{\boldsymbol{u}}_\mathrm{f} + \boldsymbol{K}_\mathrm{ff}\boldsymbol{u}_\mathrm{f} = \boldsymbol{\Phi}_\mathrm{gf}^\mathrm{T} \boldsymbol{P}_\mathrm{g}^\mathrm{ext} \tag{1b}$$

where equation (1a) is the nonlinear Newton-Euler equation of motion (b-set), representing the rigid body dynamics. The second order equation (1b) (f-set) is representing the structural

dynamics of the airframe. In equation (1a), translational velocities $\dot{\boldsymbol{v}}_\mathrm{b}$ and angular rate Ω_b of the aircraft center of mass in body axis (index b) are defined by $\dot{\boldsymbol{v}}_\mathrm{b} = [\dot{\boldsymbol{v}}_\mathrm{b,x}\ \dot{\boldsymbol{v}}_\mathrm{b,y}\ \dot{\boldsymbol{v}}_\mathrm{b,z}]^T$ and $\boldsymbol{\omega}_\mathrm{b} = [p_b\ q_b\ r_b]^T$, respectively. The structural deformation is described by the modal coordinates $\boldsymbol{u}_\mathrm{f}$, where the number of coordinates is defined to achieve sufficient accuracy for the loads calculation. This results in the modal basis defined in $\boldsymbol{\Phi}_\mathrm{gf}$. The modal properties of the airframe are characterized by mass $\boldsymbol{M}_\mathrm{ff}$, damping $\boldsymbol{B}_\mathrm{ff}$ and stiffness $\boldsymbol{K}_\mathrm{ff}$ matrices. The structural matrices originate from a reduced finite element model, derived by static reduction like the Guyan reduction [6] from a finite element model. The stiffness properties are determined for condensation points (g-set) along the loads reference axis. The transformations between the condensation points (g-set) and the rigid body dynamics respectively the flexible dynamics are defined by $\boldsymbol{\Phi}_\mathrm{gb}$ and $\boldsymbol{\Phi}_\mathrm{gf}$. The mass distribution of the aircraft is approximated by uncoupled lumped masses attached to the g-set.
The external loads $\boldsymbol{P}_\mathrm{g}^\mathrm{ext}$ consist of the aerodynamic $\boldsymbol{P}_\mathrm{g}^\mathrm{aero}$ and propulsion loads $\boldsymbol{P}_\mathrm{g}^\mathrm{prop}$. The aerodynamic loads are modeled by a panel method based on potential flow theory, i.e. the unsteady *doublet lattice method* (DLM). The aerodynamic load equation for the DLM model is defined as

$$\boldsymbol{P}_\mathrm{g}^\mathrm{aero}(k) = q_\infty \boldsymbol{T}_\mathrm{kg}^\mathrm{T} \boldsymbol{S}_\mathrm{kj} \underbrace{\boldsymbol{Q}_\mathrm{jj}(k) w_\mathrm{j}}_{\Delta c_\mathrm{p}(k)}, \tag{2}$$

in frequency domain, where q_∞ is the freestream dynamic pressure and $\boldsymbol{T}_\mathrm{kg}$ is the splining matrix. This matrix maps the displacement of the structural grid to the aerodynamic panel model and, vice versa, the aerodynamic loads to the structural grid. The matrix $\boldsymbol{S}_\mathrm{kj}$ integrates the pressure coefficients $\Delta \boldsymbol{c}_\mathrm{p}(k)$ over each panel. The pressure coefficients depend on the Aerodynamic Influence Coefficient (AIC) matrix $\boldsymbol{Q}_\mathrm{jj}(k)$ as well as the downwash $\boldsymbol{w}_\mathrm{j}$. The AIC matrix is derived for multiple reduced frequencies $k = \omega \frac{c_\mathrm{ref}}{2U_\infty}$. In order to transfer $\boldsymbol{P}_\mathrm{g}^\mathrm{aero}(k)$ from the frequency domain into the time domain, the Rational Functions Transformation by Roger [7] is applied to gain a frequency domain approximation of $\boldsymbol{P}_\mathrm{g}^\mathrm{aero}(k)$, which has a time domain representation [5].

3.1.1 Force summation method

The key objective of a gust load alleviation system is to reduce the internal loads (cut-loads) [8] $\boldsymbol{P}_\mathrm{c}$ acting within the structure during the encounter of an atmospheric disturbance. These are obtained using the force summation method (FSM) [5]. The loads $\boldsymbol{P}_\mathrm{g}$ acting at the nodes of the structural grid (g-set) result from the external loads $\boldsymbol{P}_\mathrm{g}^\mathrm{ext}$ and inertia loads $\boldsymbol{P}_\mathrm{g}^\mathrm{iner}$:

$$\boldsymbol{P}_\mathrm{g} = \boldsymbol{P}_\mathrm{g}^{ext} - \boldsymbol{P}_\mathrm{g}^\mathrm{iner} = \boldsymbol{P}_\mathrm{g}^{aero} + \boldsymbol{P}_\mathrm{g}^\mathrm{prop} - \boldsymbol{P}_\mathrm{g}^\mathrm{iner}. \tag{3}$$

Finally, the internal loads are derived from the nodal loads $\boldsymbol{P}_\mathrm{g}$ by

$$\boldsymbol{P}_\mathrm{c} = \boldsymbol{T}_\mathrm{cg} \cdot \boldsymbol{P}_\mathrm{g} \tag{4}$$

where $\boldsymbol{T}_\mathrm{cg}$ is a linear transformation from nodal loads (g-set) to cut loads (c-set). Further details on the loads are provided in [8].

3.1.2 Atmospheric disturbance by 1-cos discrete gusts

The standard scenario for the structural load analysis of a atmospheric disturbance encounter is the 1-cos discrete gust encounter defined in the certification standard CS/FAR 25.341 [9]. This disturbance wind profile is characterized by

$$v^\mathrm{1cos} = \frac{U_0}{2}\left[1 - \cos\left(\frac{\pi x_j}{H}\right)\right], \tag{5}$$

where U_0 is the design gust velocity, $\boldsymbol{x}_\mathrm{j}$ is the distance in aircraft longitudinal axis between the aerodynamic panel and the reference gust coordinate, and H is the gust gradient length. Therefore $\boldsymbol{v}^{1\cos}$ contains the disturbance time signal for each individual aerodynamic panel j.

3.2 Control synthesis models and design load cases

For design of the gust load alleviation control laws, linear state space models, which approximate the equations of motion (1a),(1b) for a long-range wide-body aircraft, are used. This requires a steady flight condition, which is a 1g horizontal flight in this case. Therefore, a thrust lever position as well as control surface deflections $\boldsymbol{u}_0$ are derived, leading to the desired flight condition $\boldsymbol{x}_0$. The linear state space model is derived at the flight point defined by $\boldsymbol{x}_0$ and $\boldsymbol{u}_0$. The inputs to the state space model consist of the control surface angle, rate and acceleration command as well as the thrust. The model delivers parameters such as rigid body velocities, angular rates and attitude as well as load factors at the center of gravity. Furthermore, acceleration and angular rate measurements are calculated close the REUs. Additionally, the internal loads at the defined monitoring stations are also within the outputs of the state space model.
Such linear state space models are derived for 54 different flight configurations varying with respect to mass configuration, aerodynamic configuration (airbrake deflected by $30°$, or clean), Mach number and altitude. The mass cases contain operation empty mass as well as light and heavy payload, also differing with respect to position of center of gravity. Additionally, mass cases for maximum take off mass are considered. Three different altitudes, $\boldsymbol{z}_{\mathrm{E,d}} = [0\ \mathrm{m}, 3000\ \mathrm{m}, 8300\ \mathrm{m}]$ are taken into account. The cruise design speed of $\mathrm{V_C} = 170\ \mathrm{m/s}$ leads to the Mach numbers $\mathbf{Ma_d} = [0.500, 0.601, 0.861]$ at the defined altitudes. These flight points resulted from previous studies investigating the flight points, where the maximum wing root bending moment due to discrete gust encounter occur. This results in 54 different configurations, as shown in Table 1, and therefore 54 state space models.
The different configurations are analyzed with respect to discrete gust encounters using the following gust gradient lengths $\mathbf{H}_\mathrm{d} = [9\ \mathrm{m}, 40\ \mathrm{m}, 76\ \mathrm{m}, 107\ \mathrm{m}]$. In combination these configurations are leading to 216 design load cases.

Table 1: Overview of the 216 design load cases

<table>
<tr><td colspan="5">Flight Configurations</td><td>Gusts</td></tr>
<tr><td rowspan="2">mass configuration</td><td colspan="3">flight points</td><td rowspan="2">trim condition</td><td rowspan="2">aerodynamic configuration</td><td rowspan="2">gust gradient H</td></tr>
<tr><td>altitude</td><td>Mach number</td><td>true airspeed</td></tr>
<tr><td rowspan="6">MCAae
MCFfe
MHAAe
MHFFe
MOOee
MTAAJ
MTFFJ
MTmMG
MZmMe</td><td rowspan="2">0 m</td><td rowspan="2">0.500</td><td rowspan="2">170.00 m/s</td><td rowspan="6">steady horizontal flight</td><td rowspan="3">clean</td><td>9 m</td></tr>
<tr><td>40 m</td></tr>
<tr><td rowspan="2">3000 m</td><td rowspan="2">0.601</td><td rowspan="2">197.34 m/s</td><td rowspan="3">airbrake out</td><td>76 m</td></tr>
<tr><td rowspan="2">8300 m</td><td rowspan="2">0.861</td><td rowspan="2">264.26 m/s</td></tr>
<tr><td>107 m</td></tr>
<tr><td>9</td><td>x</td><td>3</td><td>x</td><td></td><td>2</td><td>x 4 = 216</td></tr>
</table>

3.3 Modeling of the load-dependent actuator

The actuation subsystem simulation comprises the electro-hydraulic servo actuator (EHSA) including the associated position control loop and the local load alleviation loop. The EHSA

model including the position control loop were derived from a simulation model for a production large transport aircraft aileron actuator. Thus, the actuation model is fully representative of a state-of-the-art primary flight control actuator. This way, the dynamics and limitations of a typical primary flight control actuator are considered in the assessment of the decentralized load control concept.

The EHSA simulation is a high-fidelity model incorporating nonlinear features of the physical actuator, like servo valve hysteresis, stick/slip effects caused by piston seals, as well as actuation rate limiting. The EHSA output position is fed into the flight physics model with aerodynamic loads being fed back to the EHSA simulation. These fed back aero loads impact the dynamic performance of the EHSA, with increasing loads resulting in decreasing available maximum actuation rate. The simulation reflects the load dependent behavior of the EHSA, including stalling in case the load has reached a value when no counteracting actuator rate can be produced. The simulation rate of the physical actuator model is 20 kHz.

The EHSA position control loop is derived from state-of-the-art solutions as implemented for various serial products. The local load control loop receives local acceleration feedback and the FCC flight control demands. It also provides means for receiving and processing data on the flight state for potential usage of e.g. airspeed-depending controller gains. With the envisaged physical implementation, the distributed acceleration sensors would be hosted on the REU. The physical characteristics of these sensing elements are in a first approximation represented by delays in the simulation model. The acceleration value is provided by the flight physical model which has been expanded to provide the accelerations exactly at the locations of the REUs. The synthesis and tuning of the design of the local load controller is shown in Section 4. Implementation aspects of the controller functions hosted on the REU are reflected by discretized control loops which can be run at rates between 300 Hz and 1000 Hz.

The following figure provides an overview of the Liebherr-Aerospace Lindenberg (LLI) simulation model with its main components and interfaces to the surrounding simulation environment.

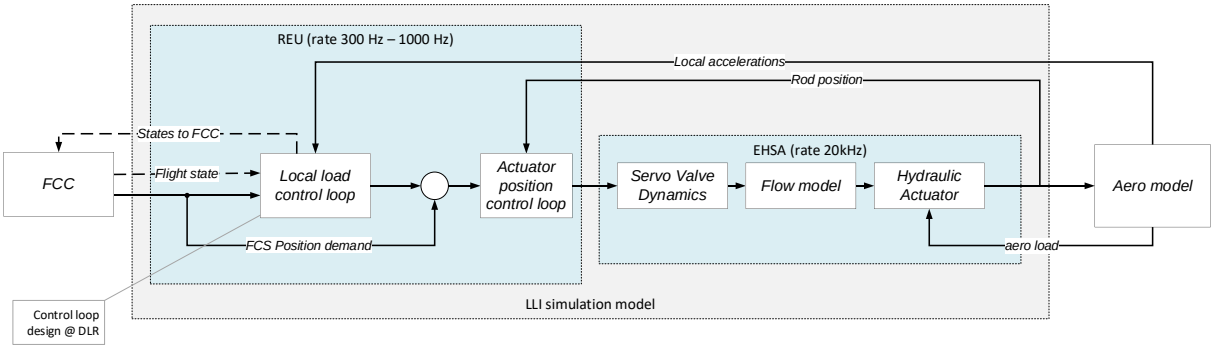

Figure 3: Scope of the LLI simulation model

4 OPTIMIZATION OF THE DECENTRALIZED CONTROL

With the concept of decentralized control and the modeling of the entire plant as decribed in Section 3, in the next step the controller is designed and then optimized. Suitable criteria are defined for the optimization to ensure high performance and stability of the controller.

4.1 Structure of the REU control function

The design of a controller offers many degrees of freedom. A suitable controller structure must therefore be selected for the decentralized concept. The controller must be able to run indepen-

dently on the REUs and should therefore not require too many inputs or be too computationally intensive. As the potential application is in aviation, the safety-specific approval requirements must also be taken into account. In particular, this means that a proven and comprehensible controller structure is used. Therefore, a controller with proportional part and integral part is used (PI). A derivative part is not used, as the controller reacts to accelerations. These acceleration signals are subjected to noise in the simulation, as they cannot be ideally measured in a real application either. A derivative part of the controller on an acceleration, which is also noisy, is not advantageous. This PI controller runs independently on each of the REUs with individual control parameters, which are subsequently determined using the modeled plant and an optimization approach.

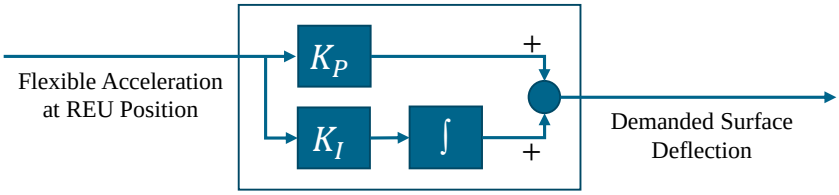

Figure 4: Controller Structure in REU

Figure 4 shows the structure of the controller. The control parameters K_P and K_I can be seen, as well as the output of the controller: the demanded surface deflection (ailerons in this case). The input are the flexible accelerations at the REU position in z-direction. The flexible accelerations are calculated with the accelerations at the REU position, minus the rigid body accelerations converted to REU position (compare Fig. 2), as these should not be suppressed by the decentralized control. If only accelerations at REU position were used, then desired accelerations such as pilot inputs would be suppressed as well.

4.2 Definition of quality criteria

The decentralized control is intended to achieve the highest possible reduction of accelerations on the wing. This also reduces the loads on the wing, such as the wing root bending moment. A maximum position and rate of the control surface must thereby not be exceeded. Excessive actuator activity is also undesirable in order to limit maintenance costs and wear, insofar as this is possible with such an active control system. The stability of the control system must also be ensured. To achieve this, criteria must be defined that express the desired behavior of the control system as precisely as possible in scalar values. In turn, these values can then be used for the optimization.

4.2.1 Performance

Two criteria are defined to evaluate the performance of the gust load alleviation control. One is the maximum flexible z-acceleration at REU position $a_{z,\,REU,\,max}$. Also, its integral over time is defined as criterion $Int_{a_{z,\,REU}} = \int |a_{z,\,REU}|\,dt$. While $a_{z,\,REU,\,max}$ takes the maximum values into account and thus ensures that the control reduces the acceleration peaks during optimization, the criterion $Int_{a_{z,\,REU}}$ ensures that the decay of the accelerations after excitation also takes place in a shorter time.

4.2.2 Limitations of the actuator

The performance of the actuator is crucial for gust load alleviation control. Of course, an actuator with unlimited speed is desirable here in order to react quickly to very short-term disturbances (such as gusts). In reality, it is a compromise between weight, economic efficiency

and possible gust load reduction, which is why the deflection and speed of the actuator are limited. In order to avoid the decentralized control being constantly in saturation, the limitations of the actuator are already taken into account in the controller design. The maximum position of the control surface δ_{max} and its maximum rate $\dot{\delta}_{max}$ are used as criteria. This type of active control places a very high load on the actuator due to the high activity of the control surfaces. The activity of the actuator is only partially described by the previous two criteria, which is why a further criterion is introduced to express the activity numerically. The integral of the control surface position $Int_\delta = \int |\delta| \, dt$ is used for this.

4.2.3 Stability

In addition to the criteria mentioned above, the stability of the control loops must always be guaranteed. For this purpose, the modulus margin of the individual controllers and the minimum damping of the entire control loop are considered.
The modulus margin Mm [10] is a stability criterion that considers the combined amplitude and phase reserve. It is particularly suitable for optimization as it reduces the number of criteria and offers the optimization algorithm fewer 'loopholes'. If the amplitude and phase reserve are considered separately, there is a possibility that a small gain amplification with a simultaneous phase shift will lead to an unstable controller. This is prevented with the modulus margin. Figure 5 shows a Nyquist plot that can be used to visualize the various stability criteria.

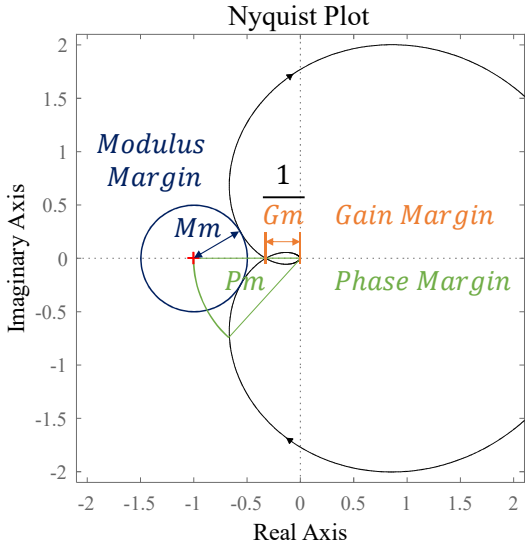

Figure 5: Nyquist plot (in black) with several stability criteria

In Figure 5 a Nyquist plot (in black) can be seen with the margins for gain and phase. Also shown is the modulus margin, which can be described as the distance of the Nyquist plot from the critical 'instability' point $(-1|0)$. A typical requirement is a modulus margin $Mm > 0.5$.

Besides the modulus margin, the minimum damping D_{min} of the closed control loop is also used as a criterion. The minimum damping must not be lower than with inactive control.

4.3 Optimization of the controller gains

The controller gains of the REUs are optimized with the primary goal of reducing the flexible accelerations of the wing. By reducing the gust-induced accelerations, the wing is deflected less and the structural loads are reduced.
The optimization process was carried out with the DLR-SR tool for Multi-Objective Parameter Synthesis (MOPS) [11] and was iterative, as shown in Figure 6.

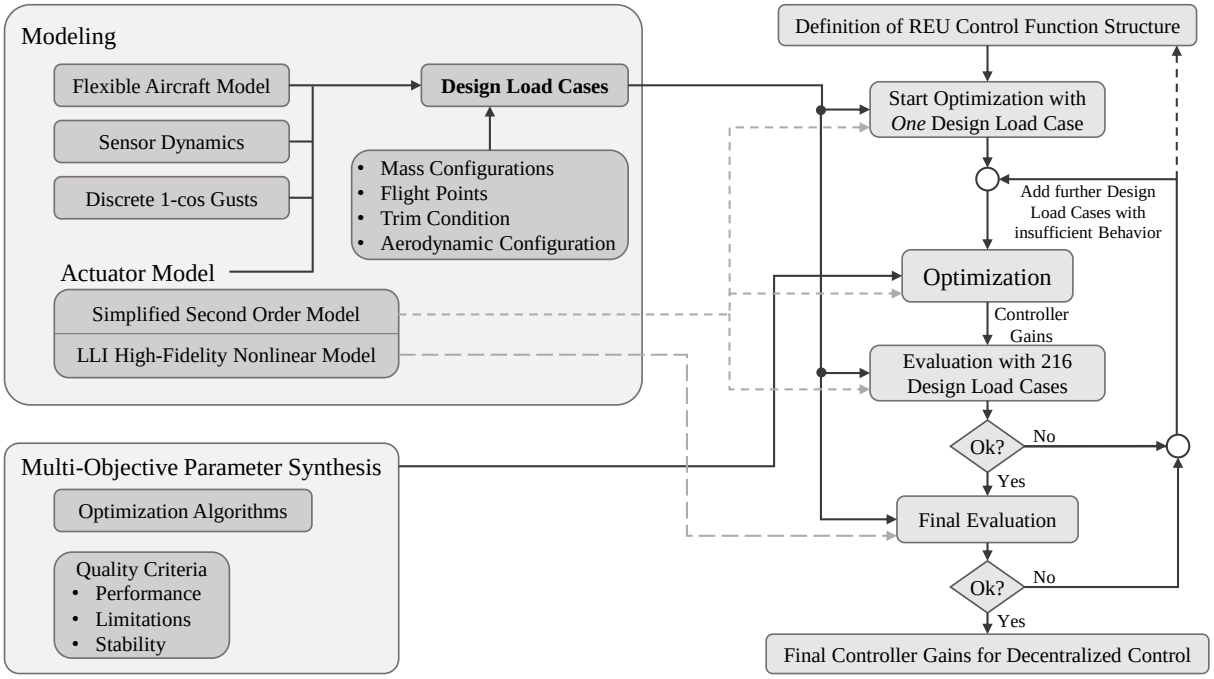

Figure 6: Process of the controller gain optimization

On the left side of Figure 6 the components are presented, which are necessary for the optimization process. These are the models, as described in Section 3, leading to the 216 design load cases, and the optimization environment MOPS, including the quality criteria to evaluate the controller performance, as defined in Section 4.2. Further information on the optimization with MOPS and the optimization algorithms can be found in [12].
On the right side the optimization process is depicted, starting with the definition of the structure of the REU control function, as described in Section 4.1. Then, one representative design load case is chosen to start the optimization with, leading to a set of controller gains. With these, all the 216 design load cases are evaluated. Cases with insufficient behavior regarding the criteria are added to the optimization. This is repeated until favorable behavior is achieved for all 216 design load cases. The use of all cases directly in the optimization would require much computing time. Therefore, this iterative process is chosen. Then, the evaluation is performed with the high-fidelity nonlinear actuator model, which is described in Section 3.3. If the results still sufficiently fulfill the quality criteria, the optimization process ends with this set of controller gains.

Due to the symmetry of the aircraft configuration, the controller gains of the REUs on the right-hand side are identical to the gains of the REUs on the left-hand side.

5 RESULTS

The evaluation is performed using the optimized controller gains of each REU and all 216 design load cases described in Section 3.2. This covers a wide range of aircraft mass distributions, flight points, control surface configurations and gust gradients. For the evaluation of the stability the second order actuator model is used, as linear transfer functions are needed for this purpose. Then, for the time domain evaluations the LLI nonlinear, high-fidelity actuator model is used. Due to the symmetry of the aircraft and the gusts, only the results of the right wing are regarded.

With regard to the stability of the control loops, the modulus margin in particular is considered. For this purpose, the Nyquist plots of all 216 design load cases are shown in a diagram. These diagrams are shown for the inner (a)) and outer REU (b)) of the right wing in Figure 7. As described in Section 4.2.3, the modulus margin can be described as the radius around the critical instability point (-1|0). It can be seen that the requirement of a modulus margin > 0.5 can be met with the optimized parameters.

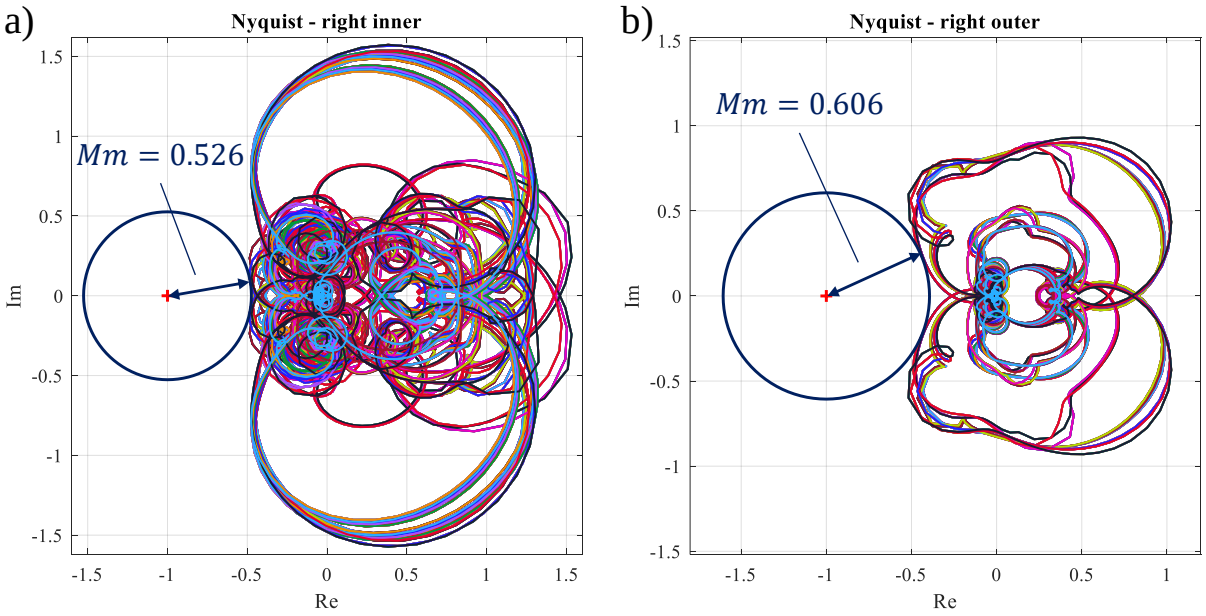

Figure 7: Nyquist plots for all 216 design load cases for both REUs of the right wing

Figure 8 shows the flexible accelerations at the outer REU for the 216 design load cases in the open-loop case in blue hues, i.e. without gust load reduction. The flexible accelerations for the design load cases with an active decentralized gust load reduction system are shown in red hues. It can be seen that the occurring accelerations are significantly reduced with the gust load reduction system. On the one hand, the maximum accelerations occurring are reduced and, on the other hand, the decay behavior of the oscillation is also significantly improved. The maximum positive accelerations are reduced by 48.4 % and the negative ones by 56.4 %.

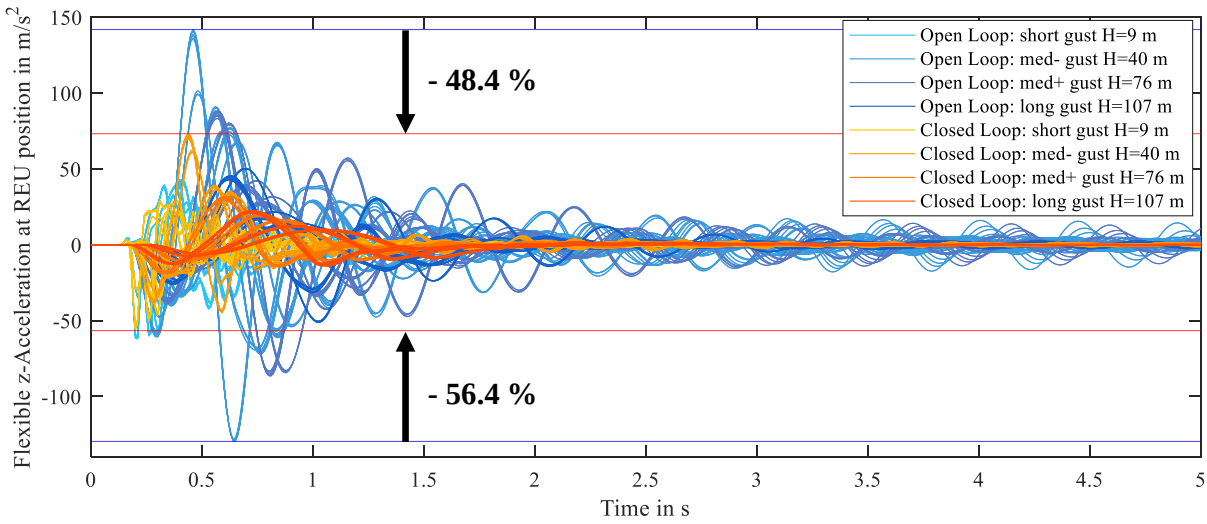

Figure 8: Flexible Accelerations at outer REU for all 216 design load cases

The reduced acceleration of the wing also reduces the gust-induced loads on the wing. This manifests itself, among other things, in a reduced bending moment at the wing root. Figure 9 shows the courses of the wing root bending moment of the 216 design load cases for the open loop case (blue) and with active control (red). It can be seen that the maximum value of the wing root bending moment is reduced by 13.7 % by the decentralized gust load reduction system.

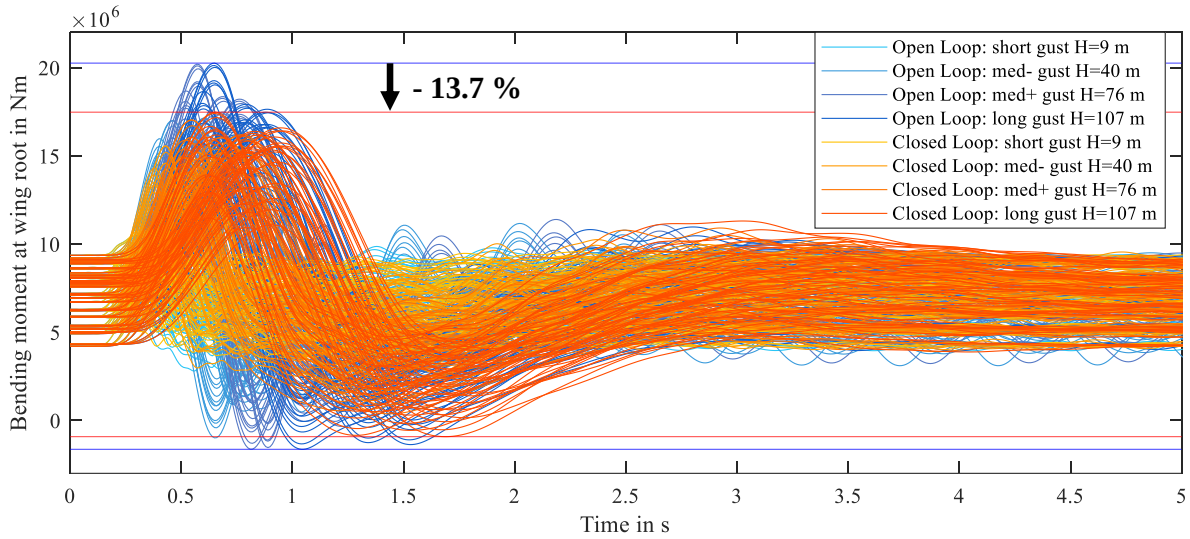

Figure 9: Wing root bending moments for all 216 design load cases

There is also a relative reduction in the maximum bending moment across the wing, starting with the value at the wing root of 13.7 %. This is followed by a reduction of 16.3 % at the height of the engine nacelle and 15.5 % in the middle section of the wing. Directly in front of the ailerons, the bending moment is still reduced by 12.0 %. These reductions are also shown graphically in Figure 10.

6 CONCLUSION

We demonstrated the design and tuning of a decentralized control system for gust load alleviation. This was performed with simulation models of the aircraft and the disturbances. The parameters of the local control laws were optimized with a multi-objective optimization approach using design criteria on a local and aircraft level. It turns out that in spite of the simple control concept considerable load alleviation is achieved. It was shown that the maximum wing root bending moment can be reduced by 13.7 %. But also the maximum bending moments across the wing can be reduced (see Fig. 10).

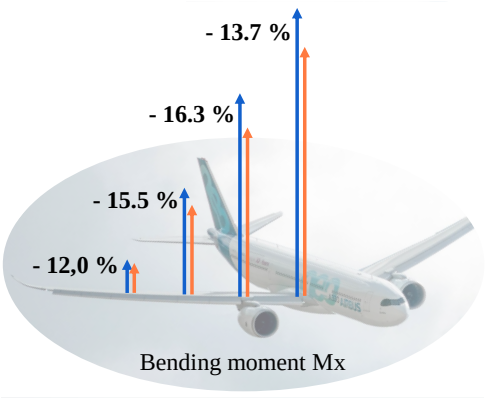

Figure 10: Reduction of maximum bending moments across wing

This analysis was performed for a model of a large passenger aircraft with a symmetric gust encounter with very promising results. Currently we are taking more complex gust scenarios into account, like asymmetric encounters, as well as continuous turbulence. In addition, interactions with other functions, like primary flight control, are addressed. The physical principle has also been validated in a wind tunnel experiment. The results will be published in [13].

7 ACKNOWLEDGMENTS

This research has received funding from the German Federal Ministry for Economic Affairs and Climate Action (BMWK) in the frame of the *LuFo VI-1 INTELWI* joint research project (FKZ: 20A1903L) that was conducted from 2020 to 2023.

8 REFERENCES

[1] Regan, C. D. and Jutte, C. V. (2012). Survey of Applications of Active Control Technology for Gust Alleviation and New Challenges for Lighter-weight Aircraft. *Tech. Mem. NASA/TM—2012–216008*.

[2] MacMartin, D. (1995). Collocated structural control: motivation and methodology. In *Proceedings of International Conference on Control Applications*. pp. 1092–1097. doi: 10.1109/CCA.1995.555912.

[3] Weber, G., Hartmann, A., Schneider, C., et al. (2021). Decentralized Load Alleviation System. In *SEE MEA (More Electric Aircraft) 2021*.

[4] Wallace, C., Schulz, S., Fezans, N., et al. (2022). Evaluation Environment for Cascaded and Partly Decentralized Multi-Rate Load Alleviation Controllers. In *33rd Congress of the International Council of the Aeronautical Sciences (ICAS) 2022*.

[5] Kier, T. and Looye, G. (2009). Unifying Manoeuvre and Gust Loads Analysis Models. In *International Forum on Aeroelasticity and Structural Dynamics (IFASD) 2009*.

[6] Guyan, R. J. (1965). Reduction of stiffness and mass matrices. *AIAA Journal*, 3(2), 380. ISSN 0001-1452. doi:10.2514/3.2874.

[7] Roger, K. L. (Ed.). *Airplane Math Modeling Methods for Active Control Design*.

[8] Wright, J. R. and Cooper, J. E. (2015). *Introduction to Aircraft Aeroelasticity and Loads*. Aerospace series. Chichester, West Sussex, United Kingdom: Wiley, second edition ed. ISBN 978-1-118-48801-0.

[9] European Union Aviation Safety Agency (2023). Certification Specifications and Acceptable Means of Compliance for Large Aeroplanes (CS-25): CS-25.

[10] Keviczky, L., Bars, R., Hetthéssy, J., et al. (2019). *Control Engineering*. Advanced Textbooks in Control and Signal Processing. Springer Nature Singapore. ISBN 9789811341144.

[11] Joos, H.-D., Bals, J., Looye, G., et al. (2002). A multi-objective optimisation-based software environment for control systems design. In *Proc. of CCA/CACSD 2002*. pp. 7–14.

[12] Michel, K. and Schallert, C. (2023). Multi-Objective Controller Optimization and Robustness Analysis by the Example of Electro-Mechanical Flight Surface Actuation. In *Aerospace Europe Conference 2023 – 10th EUCASS – 9th CEAS*.

[13] Michel, K., Stalla, F., Looye, G., et al. (2025). Demonstration of Decentralized Control for Gust Load Alleviation in a Wind Tunnel. *Submitted to AIAA SciTech 2025 Forum*.

COPYRIGHT STATEMENT